Chinese Chemical Letters 33 (2022) 2573–2578

Contents lists available at ScienceDirect

Chinese Chemical Letters

journal homepage: www.elsevier.com/locate/cclet

A 3D MIL-101@rGO composite as catalyst for efficient conversion of straw cellulose into valuable organic acid

Yuan Su[a,1], Mengchu Lu[b,1], Ruidian Su[b], Weizhi Zhou[c], Xing Xu[b,*], Qian Li[b,*]

[a] School of Mathematic and Quantitative Economics, Shandong University of Finance and Economics, Ji'nan 250014, China
[b] Shandong Key Laboratory of Water Pollution Control and Resource Reuse, School of Environmental Science and Engineering, Shandong University, Qingdao 266200, China
[c] School of Civil Engineering, Shandong University, Ji'nan 250100, China

ARTICLE INFO

Article history:
Received 17 June 2021
Revised 23 July 2021
Accepted 18 August 2021
Available online 21 August 2021

Keywords:
Straw cellulose
MIL-101(Cr)
Three-dimensional graphene
Catalystic conversion
Organic acid

ABSTRACT

Efficient conversion of straw cellulose to chemicals or fuels is an attracting topic today for the utilization of biomass to substitute for fossil resources. The development of catalysts is of vital importance. In this work, a composite catalyst metal-organic frameworks (MOFs) immobilized on three-dimensional reduced graphene oxide (3D-rGO) were synthesized by *in situ* growth of the MIL-101(Cr) within the 3D-rGO matrix. The supporting of 3D-rGO guaranteed the dispersion and acid site density of MIL-101(Cr). The MIL-101(Cr)@3D-rGO nanocomposite possesses excellent catalytic activity, stability, recyclability and is an idea catalyst for the efficient degradation of straw cellulose into formic acid (FA), acetic acid (AA) and oxalic acid (OA). A maximum FA conversion rates of 95.36% was obtained by using MIL-101(Cr)@3D-rGO(1:1) as catalyst and hydrothermal reaction at mild conditions of 200 °C for 1h in alkaline aqueous medium. The MIL-101(Cr)@3D-rGO nanocomposite can be reused with high catalytic activity without any collapse of structure or leaching of chromium.

With growing concerns about energy shortages and environment degradation, finding renewable and green energy sources as alternatives to petroleum-based productions have received worldwide attention. Conversion of biomass to chemicals or liquid fuels are attracting much interest in recent years, among which the degradation of cellulose into high value-added platform compounds is regarded as one of the most important direction. Among various of valuable biomass-derived products such as hydroxymethylfurfural (HMF), aldols and small molecule acids [1,2]. Formic acid (FA) has received much attention because it is closely related to fuel-cell-based hydrogen economy and has the potential to serve as a hydrogen generation/storage material with its high energy density. On the other hand, crops residue such as straw produced in agriculture exceed 72 millionton annually in China. Much of it was used as fuel for direct combustion which could not only arouse pollution of the environment but also cause waste of resources. Among them, wheat straw (WS), containing 40%–60% of natural cellulose, hemicelluloses and lignin, has the potential to become the plentiful raw materials source for chemical conversion to produce high value-added fuel [3].

Generally, the conversion of cellulose into platform molecules is achieved by the oxidation of carbonhydrates in the presence of catalysts. Nanoparticle catalyst, solid acid catalyst and alkali metal catalyst have shown remarkable effect [4-6]. For example, with the solid heteropoly acid $Cs_{2.5}H_{0.5}PW_{12}O_{40}$ catalyst, fructose could produces HMF with high efficiency in a two-phase system [5]. The Ru-based catalyst could convert the cellobiose and cellulose to a hexahydric alcohol with high selectivity [6]. The composite catalyst of Ir/SiO_2 and zeolite can directly convert microcrystalline cellulose into *n*-butane [7]. However, these reactions are generally heterogeneously catalyzed. And there are few studies on the efficient catalytic degradation of cellulose to small molecule acids. The presence of repeated 1,4-β glycosidic bonds and complex hydrogen bonding networks in cellulose make them very difficult to dissolve, thus reducing the efficiency of heterogeneous catalysis. Recently, studies have shown that cellulose can be dissolved in ionic liquid or alkaline aqueous solutions, and then can be homogeneously degraded to HMF or small molecular acids, which depends on the catalyst system [8]. But the high conversion efficiency and selectivity of product should be improved.

Metal-organic frameworks (MOFs) are a kind of organic-inorganic hybrid materials with metal ions or metal clusters as

* Corresponding authors.
E-mail addresses: xuxing@sdu.edu.cn (X. Xu), qianli@sdu.edu.cn (Q. Li).
[1] These authors contributed equally to this work.

https://doi.org/10.1016/j.cclet.2021.08.078
1001-8417/

nodes and organic ligands as skeletons. They have great advantages in controllable regular nanochannel structure, large specific surface area and porosity, and easy functionalization compared with traditional inorganic and organic materials. As a result, there has been widespread interest in the fields of gas storage and separation, chemical sensing, drug delivery, and catalysis [9-11]. In particular, owing to the rich Lewis acid sites based on unsaturated metal centers, MOFs are regarded as promising catalytic materials [12]. However, MOFs also have some shortcomings including poor water resistance and difficulty in recovery, which limit their widespread application. Among various MOFs, MIL-101(M) possesses a rigid mesoporous and microporous cage structure with a very large specific surface area, in which $MO_4(OH)_2$ (M = Cr, Fe, Al) octahedron and terephthalic acid (BDC) are bridged in space. The special matrix of MIL-101(M) ensures its excellent hydrothermal stability and chemical stability, and has a greater advantage in adsorption and catalysis than other MOFs [13]. Moreover, the catalytic performance of MIL-101 is mainly derived from the unsaturated sites of surface metals. Compared with the Fe-based and Al-based MILs materials, MIL-101(Cr) has more unsaturated sites and stronger stability, therefore, it has great application potential especially in the field of heterogeneous catalysis.

In addition, in order to solve the defects of the material and ensure the catalytic activity of the material, it is particularly important to fix the MOFs on a suitable solid support [14]. Graphene is an excellent carrier material with high specific surface area, stable thermochemical properties, strong mechanical strength and structural adjustability [15]. However, the existence of van der Waals forces and π-π superposition between graphene sheets tend to cause its recombination and aggregation, resulting in a significant decrease in specific surface area [16]. Assembling two-dimensional graphene to create a three-dimensional graphene structure could overcome these defects and provide the possibility for immobilizing MOFs nanoparticles within its matrix [17]. Meanwhile, the adhesion of the internal solid particles, especially MOFs with caged skeleton, can also support the 3D structure and prevent the agglomeration of the graphene sheets. Therefore, the combination of the two materials not only solves the problems of difficult recovery of MOFs and easy agglomeration of graphene, but also contributes to the dispersion of active sites on MOFs, which ensure the sufficient contact of catalyst and reactants to improve catalytic efficiency [18,19].

In this paper, MIL-101(Cr) was *in-situ* synthesized within the 3D-rGO matrix to form MIL-101(Cr)@3D-rGO nanocomposite. Then, it was used as catalyst to efficiently convert straw cellulose to valuable organic acid in a homogeneous alkaline solution. Furthermore, the appropriate hydrothermal conditions of the conversion reactions were systematically evaluated, and a high selectivity and yield of formic acid was obtained.

The synthesis process of MIL-101(Cr)@3D-rGO(n) (n represents the mass ratio of MIL-101(Cr) and 3D-rGO) is shown in Fig. 1a. The SEM image of MIL-101(Cr) (Fig. 1b) showed that the prepared MIL-101(Cr) possessed a regular crystal morphology with a diameter of about 300–400 nm. The internal defects and wrinkles of 3D-rGO were clearly observed (Fig. 1c). SEM image of MIL-101(Cr)@3D-rGO(1:1) (Fig. 1d) clearly showed that plenty of MIL-101(Cr) nanocrystalline were formed inside the network, almost completely occupied the defects and wrinkles of the 3D-rGO surface, which demonstrated that MIL-101(Cr) was uniformly attached within the 3D-rGO grid. Compared with the SEM image of MIL-101(Cr)@3D-rGO(1:2) (Fig. S1 in Supporting information), it can be seen that MIL-101(Cr) in MIL-101(Cr)@3D-rGO(1:1) was more fully attached inside 3D-rGO. The element composition and distribution (C, O, N, Cr) of MIL-101(Cr)@3D-rGO(1:1) were detected in SEM element mapping (Fig. 1e) and elemental analysis (Fig. 1f). The C were observed uniformly distributed within the composite, showing the skeleton of 3D-rGO. The O and Cr images could fit into each other and O atoms were distributed near the Cr atom positions, pointing to Cr-O. The Cr/O atom ratio was about 1:1, which was corresponding to the elemental composition of MIL-101(Cr). The scattered N atoms were attributed to the $Cr(NO_3)\cdot 9H_2O$ during the preparation. And visible images of EDS mapping results confirmed that MIL-101(Cr) were successfully synthesized and dispersed uniformly within the 3D-rGO matrix. The TEM image of MIL-101(Cr)@3D-rGO(1:1) (Fig. S2 in Supporting information) also showed the regular crystal morphology of MIL-101(Cr).

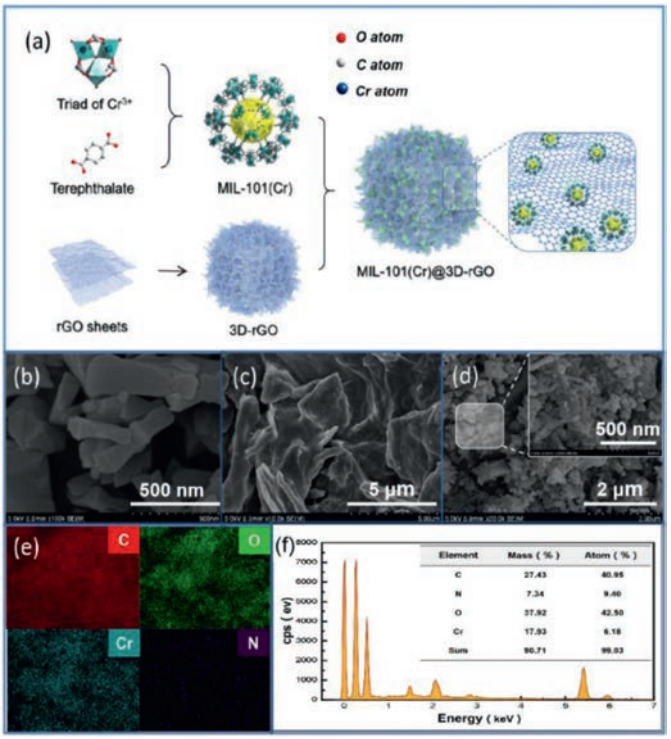

Fig. 1. Preparation flow chart of MIL-101(Cr)@3D-rGO (a). SEM images of MIL-101(Cr), 3D-rGO and MIL-101(Cr)@3D-rGO(1:1) (b-d); SEM element mapping of MIL-101(Cr)@3D-rGO(1:1) (e). Elemental analysis of MIL-101(Cr)@3D-rGO(1:1) (f).

The XRD patterns of 3D-rGO, MIL-101(Cr) and MIL-101(Cr)@3D-rGO composite were exhibited in Fig. 2a. For 3D-rGO pattern, a distinct diffraction peak appeared near 21.50°, which was consistent with the corresponding surface (002) of 3D-rGO. The main peaks of MIL-101(Cr) were recorded at 5.82°, 8.33°, 9.02°, 16.39°, corresponding to (531), (882), (911), (311) of standard MOFs, respectively [20]. For the MIL-101(Cr)@3D-rGO composite, both characteristic peaks of MIL-101(Cr) and 3D-rGO were detected indicating that the addition of 3D-rGO would not affect the crystal structure of MIL-101(Cr). A stronger characteristic peak was observed as the increasing of the content of MIL-101(Cr) in the composite.

The FT-IR spectrum of the catalysts were depicted in Fig. 2b. The bands around 748 cm^{-1} were related to the deformation vibration of C–H. A adsorption band appeared around 1015 cm^{-1} was assigned to the C–O stretching. And the bands at 1348 cm^{-1} could be attributed to –OCO group from the dicarboxylate linker. The peaks observed around 1507 cm^{-1} and 1620 cm^{-1} were assigned to aromatic C=C stretches and structural water molecules, respectively [21]. It can be seen that the composite material has a good characteristic peak and the addition of 3D-rGO does not affect the formation and structure of MIL-101(Cr).

The NH_3-TPD curve is used to characterize the acidity of the composite catalyst surface. From Fig. 2c, it can be observed that two different types of 3D-rGO dosing compound catalysts

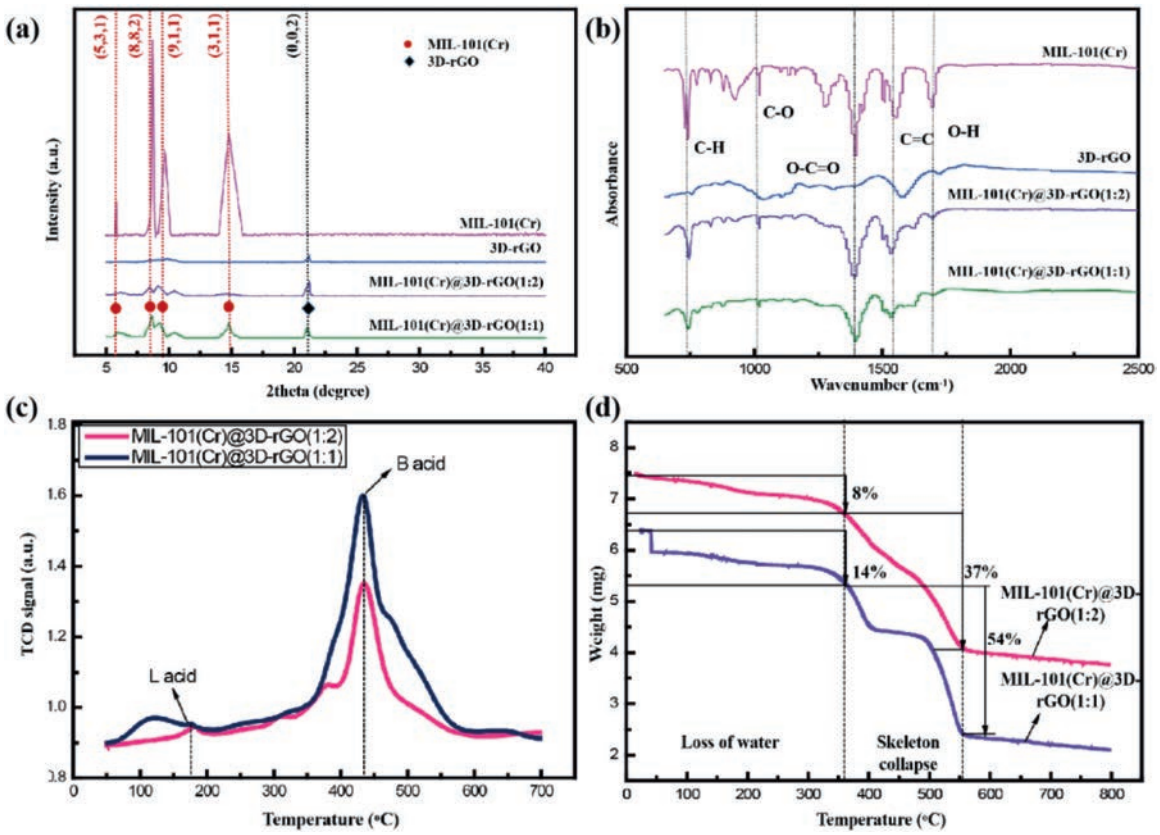

Fig. 2. XRD patterns (a) and FTIR spectra (b) of MIL-101(Cr), 3D-rGO MIL-101(Cr)@3D-rGO(1:1) and MIL-101(Cr)@3D-rGO(1:2); NH_3-TPD curve (c) of MIL-101(Cr)@3D-rGO(1:1) and MIL-101(Cr)@3D-rGO(1:2); TGA curve (d) of MIL-101(Cr)@3D-rGO(1:1) and MIL-101(Cr)@3D-rGO(1:2).

had detected acid sites with different strengths, of which MIL-101(Cr)@3D-rGO(1:1) possessed a stronger Bronsted acidic site than MIL-101(Cr)@3D-rGO(1:2). The difference in the strength of the Lewis acid sites between the two composites was not large, which was attributed to the higher proportion of MIL-101(Cr) in MIL-101(Cr)@3D-rGO(1:1) composites, of which had more activated Cr acid sites. NH_3-TPD curve confirmed that the composite material was an acidic catalyst and MIL-101(Cr)@3D-rGO(1:1) had a stronger acidic site.

The TGA curve of the composite material is shown in Fig. 2d, reflecting the thermal stability of the material. The weight loss of the composite material was mainly divided into three stages. The first stage was 20–360 °C, the weight loss at this stage was due to removal of trace water on the surface of the material (8 wt% for MIL-101(Cr)@3D-rGO(1:1), 14 wt% for MIL-101(Cr)@3D-rGO(1:2)). The second stage occurred at 360–550 °C, the weight loss at this stage is attributed to the collapse skeleton of the composite catalyst caused by the removal of the material skeleton linker (terephthalic acid). The third stage took place when the temperature was higher than 550 °C, of which the remaining weight was assigned to chromium oxide after combustion. In addition, the weight loss of MIL-101(Cr)@3D-rGO(1:1) and MIL-101(Cr)@3D-rGO(1:2) are 67 wt% and 49 wt%, respectively, which proved that as the proportion of 3D-rGO increased, the thermal stability of the composite material was enhanced. At the same time, the composite material can keep the skeleton intact under 360 °C, which can be used for the catalytic reaction of cellulose.

The XPS survey spectra of the as-prepared MIL-101(Cr)@3D-rGO(1:1) were detected in Fig. S3 (Supporting information). The photoelectron peaks of main elements on the surface of MIL-101(Cr)@3D-rGO(1:1) appeared at the binding energies of 284 eV (C 1s), 534 eV (O 1s) and 578 eV (Cr 2p), respectively, confirming the presence of MIL-101(Cr) on the framework of 3D-rGO. The binding energy at 289.1 eV and 284.5 eV of C 1s can be assigned to C=O and C=C, respectively. Among them, the C=C peak is mainly attributed to 3D-rGO, and the C=O peak is mainly MIL-101(Cr). The presence of hydroxyl and epoxy C–O was not observed at 286.5 eV, indicating that the reduction effect of 3D-rGO was relatively obvious and the network composition of graphene was mainly C=C. The Cr 2p XPS spectrum showed two main peaks appeared at 586.97 eV and 577.10 eV corresponding to Cr $2p_{1/2}$ and Cr $2p_{2/3}$, respectively, confirming the embedded Cr in MIL-101(Cr) [22]. The binding energy of 531.5 eV was due to the coordination of Cr atom with the carboxyl oxygen to form Cr–O. The XPS results showed that MIL-101(Cr) was successfully *in situ* synthesized within 3D-rGO matrix. The Raman spectroscopy spectrum of the as-prepared MIL-101(Cr)@3D-rGO(1:1) was shown in Fig. S4 (Supporting information). The characteristic D band at 1348 cm^{-1} was the disordered vibration peak of graphene, indicating the exist of defect on the surface of 3D-rGO. The main characteristic peak G of graphene at 1583 cm^{-1} was caused by the in-plane vibration of sp^2 carbon atoms. The peaks of 2590 cm^{-1} and 2700 cm^{-1} are 2D bands of graphene, which is a combination of G' peak and D' peak. The I_D/I_G of MIL-101(Cr)@3D-rGO is 1.04, indicating that there are more defects in 3D-rGO for MIL-101(Cr) synthesis *in situ*.

The pore sizes and specific surface areas of different as-prepared catalysts samples were measured and shown in Fig. S5 (Supporting information) and Table S1 (Supporting information). MIL-101(Cr) had a high N_2 adsorption capacity and exhibited a mesoporous structure with a pore diameter of 4.728 nm, while 3D-rGO was macroporous and the average pore diameter was 2.420 μm. Meanwhile, the MIL-101(Cr)@3D-rGO exhibited a significant decrease of porous surface area with the increase of MIL-101(Cr) loading levels compared with MIL-101(Cr) (2575 m^2/g) and 3D-rGO

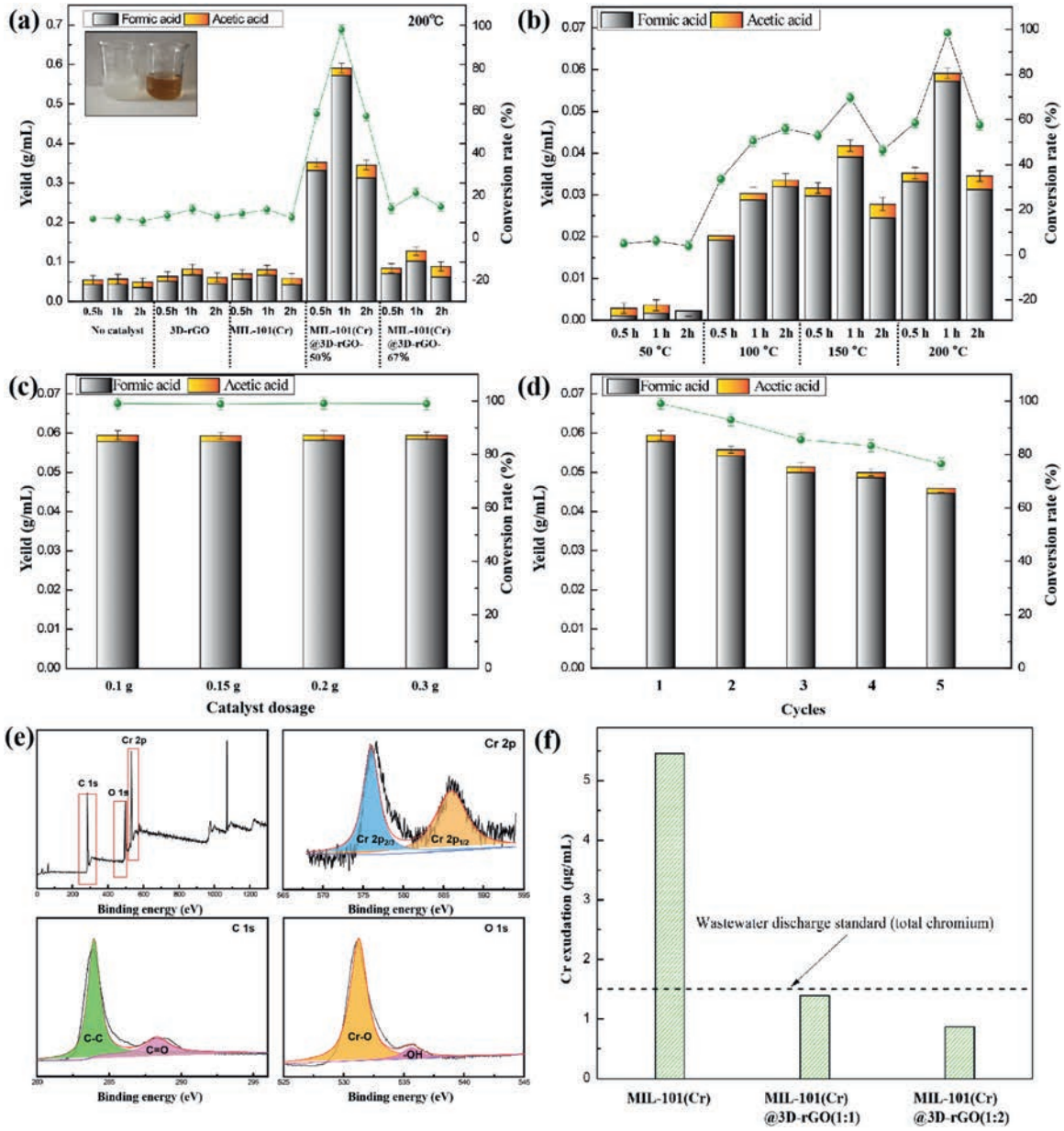

Fig. 3. Catalytic degradation of cellulose by different catalysts (reaction conditions were 200 °C, 1 h, 0.1 g of catalyst dosage) (a). Effect of reaction time and reaction temperature of MIL-101(Cr)@3D-rGO(1:1) on cellulose conversion products (b). Effect of the catalyst dosage on the conversion products of cellulose (reaction conditions were 200 °C, 1 h) (c). Circulation experiment of MIL-101(Cr)@3D-rRGO(1:1) catalyst (d). XPS spectrum of the recovered MIL-101(Cr)@3D-rGO(1:1) composite catalyst after 5 cycles of experiment (e). Cr content in leachate of different catalysts (f).

(1774 m^2/g). The appreciable decreases in surface area indicated that the pore surface of 3D-rGO and MIL-101(Cr) were presumably occupied by each other and the cage structure MIL-101(Cr) was successfully interwoven with the 3D network of rGO. The porous structure of MIL-101(Cr)@3D-rGO facilitated full exposure of the acidic sites of Cr, which greatly enhanced their contact with the cellulose solution penetrating into the 3D-rGO matrix and thus improved catalytic property for cellulose conversion.

The cellulose conversion performance catalyzed by four composite catalysts were shown in Fig. 3a. The target product was small molecule acid such as FA and AA, which could be directly detected by HPLC. It could be observed that the all as-prepared catalysts had obvious catalytic property for cellulose degradation, of which MIL-101(Cr)@3D-rGO(1:1) was the best. The product concentration of FA obtained from the degradation of cellulose for 1 h catalyzed by different materials was 0.0044 g/mL for no catalyst, 0.0067 g/mL for pure MIL-101(Cr), 0.0062 g/mL for pure 3D-rGO, 0.0572 g/mL for MIL-101(Cr)@3D-rGO(1:1) and 0.0102 g/mL for MIL-101(Cr)@3D-rGO(1:2), respectively. According to the original content of cellulose in the uniform cellulose solution (0.06 g/mL), the FA conversion rates catalyzed by different catalysts were calculated to be 7.3%, 11.1%, 10.3%, 95.4% and 16.9%, respectively. Similarly, the product concentration and conversion rates of AA were 0.0013, 0.0014, 0.0015, 0.0019, 0.0026 g/mL and 2.1%, 2.3%, 2.4%, 3.1%, 4.3%, respectively. Without catalyst, the total conversion rates of obtained FA and AA was only 9.40%, and the HPLC peak (Fig. S6 in Supporting information) was relatively complicated indicating that there were many other by-products. When the degradation was catalyzed by pure 3D-rGO and MIL-101(Cr), the amount of FA was still low, while the conversion rates of AA was increased slightly and the total conversion rates of FA and AA was 13.60% and 13.45%, respectively. For MIL-101(Cr)@3D-rGO(1:1), the conversion

rates of FA had an amazing increase to reach a maximum of 95.35% while the total conversion rates of all the products reached 98.48%. This indicated that the composite material with proper amount of 3D-rGO and MIL-101(Cr) could present a synergistic effect, with which the cellulose solution would be converted to FA efficiently. In the composite catalyst, MIL-101(Cr) promoted cellulose conversion to FA and the addition of an appropriate amount of 3D-rGO inhibited the production of by-products [17]. Moreover, an appropriate amount of 3D-rGO doping in the composite catalyst could contribute to the dispersion of MIL-101(Cr), making the acidic site of Cr in MIL-101(Cr) sufficiently contact with the cellulose alkaline solution. However, when the 3D-rGO was excessively doped, the acidic sites of Cr in the composite catalyst reduced, which is insufficient for the efficient degradation of cellulose and resulted in the conversion rates of FA and the total conversion rates of cellulose catalyzed by MIL-101(Cr)@3D-rGO(1:2) drastically dropped to 16.99% and 21.26%. Therefore, the MIL-101(Cr)@3D-rGO(1:1) composite possessed the best degradation rate and selectivity for the conversion of homogeneous cellulose. The comparation of the cellulose conversion performance catalyzed by the as-prepared MIL-101(Cr)@3D-rGO(1:1) with the other reported catalysts were listed in Table S2 (Supporting information). It can be seen that MIL-101(Cr)@3D-rGO(1:1) can efficiently decompose cellulose into a small molecular acid in an alkaline system at a relatively mid temperature and has great advantages in cellulose conversion reaction.

The effect of reaction time and temperature on cellulose degradation products were described in Fig. 3b. As the time increased from 0.5 h to 2 h, the conversion rates of FA at 50 °C and 100 °C was continuously increased from 1.883% and 31.83% to 3.850% and 53.33%, respectively. When the degradation temperature rises to 150 °C and 200 °C, the produced FA conversion rates reached maximum at 1 h. Continued to prolong reaction time will result in a decrease in FA production, which was attributed to the decomposition of FA into carbon dioxide and hydrogen at temperatures above 150 °C. It is obvious that the hydrolysis temperature is the dominant influencing factor to convert cellulose into FA using MIL-101(Cr)@3D-rGO(1:1) as catalyst, whereas reaction time has little effect [23]. But for AA, the conversion rates did not change significantly with hydrolysis temperature or time, which remained at around 4% and reached a maximum of 6.36% at 50 °C, 2 h (Figs. S7-S9 in Supporting information). It is clear that in the presence of the as-prepared composite catalyst, the conversion rate of FA could be greatly improved under certain time and temperature conditions, which implies that we can achieve high conversion selectivity of FA by adjusting hydrolysis temperature and time using MIL-101(Cr)@3D-rGO(1:1) as catalyst.

The effect of the amount of catalyst on the degradation of cellulose was shown in Fig. 3c. As the dosage of the catalyst increasing, the conversion rates of FA enhanced slightly, while the conversion rates of AA declined, resulting in the overall change exceed no more than 1%, which indicated that the dosage of the catalyst had slight impact on cellulose conversion.

Recyclability is one of the criteria for evaluating the pros and cons of the catalyst. The composite of MIL-101(Cr)@3D-rGO not only showed excellent catalytic property, but also exhibited more conducive to recycling. Thus, cycle experiment were conducted to evaluate the reusability MIL-101(Cr)@3D-rGO and the results were shown in Fig. 3d. After repeated usages for 3 times, the conversion rates of FA decreased slightly from 95.05% to 85.16% and the total conversion rates decreased by 9.89%. Repeated catalytic processes may cause the MIL-101(Cr) acidic sites to be entrapped by carbon deposits, resulting in a decrease in catalytic performance. However, after repeated use of four times, the total conversion rates of small molecule acid is still 83.26%, which exhibited the excellent recycling property of the as-prepared composite catalyst. Fig. 3e showed the XPS spectra of the composite catalyst after five cycles

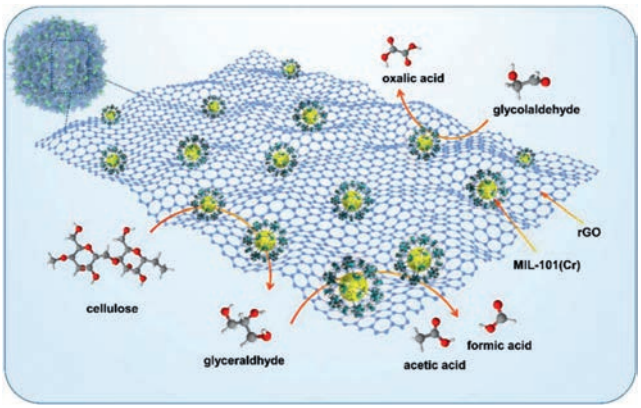

Fig. 4. The potential degradation pathways of cellulose.

experiments, compared to the XPS pattern of the catalyst before the catalytic experiment (Fig. S3), the Cr $2p_{2/3}$ peak at 577.10 eV and the C=O peak at 289.1 eV showed a slight decrease. This is attributed to the fact that after the catalyst is catalyzed, some carbon deposits adhere to the surface of the material and affect the catalytic strength of the acidic sites of Cr. The newly occurring hydroxyloxy peak at 536.23 eV may be derived from a cellulose alkaline solution [24,25].

To evaluated the stability and environmental safety of the composite catalyst, the emission of chromium during the reaction process was determined (Fig. 3f). When the pure MIL-101(Cr) was used as catalyst, a large amount of chromium ion leakage was detected. But for MIL-101(Cr)@3D-rGO, chromium ion leaching of the composite catalyst is significantly reduced with the increase of the proportion of 3D-rGO, and the chromium concentrations were lower than the national wastewater discharge standard (GB-8978–1996). So, the composite with 3D-rGO not only enhances the catalytic performance of the catalyst, but also enhances the stability of MIL-101(Cr).

Since cellulose is formed by the linkage of glucose through a 1,4-β-glycosidic bond through hydrogen bonding, there are repeated 1,4-β-glycosidic bonds and complex hydrogen bonding networks inside the cellulose, which limits the dissolution and degradation of cellulose. In this study, after dissolving cellulose in an alkaline aqueous solution with sodium hydroxide solution, each cellulose chain is surrounded by sodium hydroxide, which makes the hydrogen bond network inside the cellulose being destroyed [26]. Thus, as the catalyst is present, the cellulose macromolecule is decomposed into small molecule glucose under the action of Cr acidic site. In the catalytic process, Cr acid site of the composite catalyst accepts electrons, the glucose molecule loses electrons and the chain is progressively decomposed to glycolaldehyde, glyoxylic acid, oxalic acid and finally obtain FA. Or, glucose is converted to glycerol by hydrolysis, then AA was obtained by further hydrolysis through levulinic acid. The potential conversion pathways of cellulose was shown in Fig. 4 and Fig. S10 (Supporting information).

In the present research, a new composite catalyst MIL-101(Cr)@3D-rGO(1:1) was synthesized by *in-situ* synthesis and used for the efficient degradation and conversion of wheat straw cellulose. The MIL-101(Cr) with about 300–400 nm were tightly wrapped inside the 3D-rGO matrix and the acidic site of Cr provided a catalytic possibility for cellulose degradation. When the cellueous was catalyzed by MIL-101(Cr)@3D-rGO(1:1) at 200 °C for 1 h, an ultra-high FA conversion rate (95.36%) could be obtained. Compared with the present catalysts, MIL-101(Cr)@3D-rGO prepared in this study could possess great potential in the energization of biomass.

Declaration of competing interest

The authors declare that they have no known competing financial interests or personal relationships that could have appeared to influence the work reported in this paper.

Acknowledgments

This work was supported by the National Natural Science Foundation of China (Nos. U1906221 and 52070121). This work was also supported by grants from the Major Program of Shandong Province Technological Innovation Project (No. 2020CXGC011403).

Supplementary materials

Supplementary material associated with this article can be found, in the online version, at doi:10.1016/j.cclet.2021.08.078.

References

[1] L. Zhang, Y. Tian, Y. Wang, et al., Chin. Chem. Lett. 32 (2021) 2233–2238.
[2] Z. Tang, J.H. Su, Carbohyd. Res. 481 (2019) 52–59.
[3] T. Luo, H. Huang, Z. Mei, et al., Chin. Chem. Lett. 30 (2019) 1219–1223.
[4] C. Yuan, X. Wang, X. Yang, et al., Chin. Chem. Lett. 32 (2021) 2079–2085.
[5] Q. Zhao, L. Wang, S. Zhao, Fuel 90 (2011) 2289–2293.
[6] G.Z. Wang, X.F. Tan, H. Lv, Ind. Eng. Chem. Res. 55 (2016) 5263–5270.
[7] L. Yan, J.D. Xu, T.T. Duan, B. Zhao, Y. Fan, J. Taiwan Inst. Chem. E 99 (2019) 201–206.
[8] D. Fang, C.N. Jiang, J. Chem. Sci. 125 (2013) 751–754.
[9] Y.P. Xia, C.X. Wang, M.H. Yu, X.H. Bu, Chin. Chem. Lett. 32 (2021) 1153–1156.
[10] M. Zhu, Y. Liu, M. Chen, et al., Chin. Chem. Lett. 31 (2020) 2683–2688.
[11] M. Rimsha, I. Naseem, N. Tayyaba, Electrochim. Acta 255 (2017) 195–204.
[12] Y. Li, M.Z. Wu, D.M. Chen, Mol. Catal. 477 (2019) 110542–110550.
[13] J. Han, Y. Wang, J. Wan, Y. Ma, Environ. Sci. Pollut. Res. 26 (2019) 15345–15353.
[14] J. Chen, R. Liu, Y. Guo, ACS Cataly. 5 (2015) 722–733.
[15] H.K. Li, H.L. Ye, X.X. Zhao, et al., Chin. Chem. Lett. 32 (2021) 2851–2855.
[16] Y. Shang, Xi. Duan, S. Wang, Q. Yue, B. Gao, X. Xu, Chin. Chem. Lett. 33 (2022) 663–673.
[17] P. Huang, L. Yan, Chinese J. Chem. Phys. 29 (2016) 742–748.
[18] M. Jahan, Z. Liu, K.P. Loh, Adv. Funct. Mater. 23 (2013) 5363–5372.
[19] Y. Chen, B. Yin, Z. Yu, N. Liang, Diam. Relat. Mater. 97 (2019) 107508–107515.
[20] Y. Zheng, F.C. Chu, B. Zhang, J. Yan, Y.L. Chen, Micropor. Mesopor. Mat. 263 (2018) 71–76.
[21] R. Bulánek, P. Čičmanec, J. Kotera, I. Boldog, Catal Today 324 (2019) 106–114.
[22] Y. Li, S.F. Li, Int. J. Hydrogen Energ. 4 (2019) 10433–10441.
[23] L. Yan, J.D. Xu, T.T. Duan, B. Zhao, Y. Fan, J. Taiwan Inst. Chem. 99 (2019) 201–206.
[24] Y. Kojima, M. Takayasu, M. Toma, S. Koda, Ultrason. Sonochem. 51 (2019) 419–423.
[25] L. Nirumand, S. Farhadi, A. Zabardasti, A. Khataee, Ultrason. Sonochem. 42 (2018) 647–658.
[26] A.Sharma M.Thakur, V. Ahlawat, Mater. Sci. Energy Technol. 3 (2020) 328–334.